REPORT DOCUMENTATION PAGE

Form Approved OMB NO. 0704-0188

1. REPORT DATE (DD-MM-YYYY)	2. REPORT TYPE	3. DATES COVERED (From - To)
01-09-2014	Conference Proceeding	-

4. TITLE AND SUBTITLE
Numerical analysis of modal instability onset in fiber amplifiers

5a. CONTRACT NUMBER
W911NF-12-1-0450

5b. GRANT NUMBER

5c. PROGRAM ELEMENT NUMBER

6. AUTHORS
Benjamim Ward

5d. PROJECT NUMBER

5e. TASK NUMBER

5f. WORK UNIT NUMBER

7. PERFORMING ORGANIZATION NAMES AND ADDRESSES
University of Central Florida
12201 Research Parkway, Suite 501

Orlando, FL 32826 -3246

8. PERFORMING ORGANIZATION REPORT NUMBER

9. SPONSORING/MONITORING AGENCY NAME(S) AND ADDRESS (ES)
U.S. Army Research Office
P.O. Box 12211
Research Triangle Park, NC 27709-2211

10. SPONSOR/MONITOR'S ACRONYM(S)
ARO

11. SPONSOR/MONITOR'S REPORT NUMBER(S)
62119-EL-HEL.13

12. DISTRIBUTION AVAILIBILITY STATEMENT
Approved for public release; distribution is unlimited.

13. SUPPLEMENTARY NOTES
The views, opinions and/or findings contained in this report are those of the author(s) and should not contrued as an official Department of the Army position, policy or decision, unless so designated by other documentation.

14. ABSTRACT
Numerical analysis of the onset of modal instability in fiber amplifiers is presented. Specifically calculations of the evolution of the intensity fluctuation spectrum along the fiber for a sampling point offset from the core center are presented for different instability onset conditions. These include seeding with LP01 only, seeding with LP01 and LP11 at the same frequency, seeding with LP01 and LP11 at offset frequencies, and seeding taking quantum shot noise into account. The position dependent spectra are shown to be very similar for each of these cases suggesting a common instability mechanism.

15. SUBJECT TERMS
Fiber amplifiers, non-linear effects, thermal effects, power scaling, fiber lasers, modal instability, stimulated thermal Rayleigh scattering

16. SECURITY CLASSIFICATION OF:			17. LIMITATION OF ABSTRACT	15. NUMBER OF PAGES	19a. NAME OF RESPONSIBLE PERSON
a. REPORT	b. ABSTRACT	c. THIS PAGE			Rodrigo Amezcua Correa
UU	UU	UU	UU		19b. TELEPHONE NUMBER 407-823-6853

Report Title

Numerical analysis of modal instability onset in fiber amplifiers

ABSTRACT

Numerical analysis of the onset of modal instability in fiber amplifiers is presented. Specifically calculations of the evolution of the intensity fluctuation spectrum along the fiber for a sampling point offset from the core center are presented for different instability onset conditions. These include seeding with LP01 only, seeding with LP01 and LP11 at the same frequency, seeding with LP01 and LP11 at offset frequencies, and seeding taking quantum shot noise into account. The position dependent spectra are shown to be very similar for each of these cases suggesting a common instability mechanism.

Conference Name: SPIE Photonics West 2014

Conference Date: March 11, 2014

Numerical analysis of modal instability onset in fiber amplifiers

Benjamin G. Ward*[a]
[a]Department of Physics, 2354 Fairchild Dr. Ste. 2A31, USAF Academy, CO 80840

ABSTRACT

Numerical analysis of the onset of modal instability in fiber amplifiers is presented. Specifically calculations of the evolution of the intensity fluctuation spectrum along the fiber for a sampling point offset from the core center are presented for different instability onset conditions. These include seeding with LP01 only, seeding with LP01 and LP11 at the same frequency, seeding with LP01 and LP11 at offset frequencies, and seeding taking quantum shot noise into account. The position dependent spectra are shown to be very similar for each of these cases suggesting a common instability mechanism.

Keywords: Fiber amplifiers, non-linear effects, thermal effects, power scaling, fiber lasers, modal instability, stimulated thermal Rayleigh scattering

1. INTRODUCTION

Modal instability limits the diffraction-limited average power output of fiber amplifiers. Many experimental and theoretical studies of this phenomenon have established inter-modal coupling due to thermally-induced refractive index grating that is phase shifted from the instantaneous optical interference pattern as the cause of the instability. However, contradicting reports on the cause of the phase shift have yet to be resolved. One proposed cause is the amplification of frequency-shifted noise through stimulated thermal Rayleigh scattering (STRS) [1]. This leads to steady-state inter-modal coupling along the length of the amplifier resulting in periodic fluctuations in the output intensity profile. An alternate proposed instability mechanism is based on non-adiabatic power coupling caused by strong quasi-static grating with contributions from pump or signal noise [2]. Furthermore, instability has been observed in simulations in the absence of a frequency offset [3-4].

Experimental measurements offer limited insight into the physical foundation of modal instability because the available data pertain only to time dependent output optical intensity profiles while both of the proposed instability mechanisms rely on temperature and optical profile variations along the fiber as well as in time. Numerical models enable full examination of the spatial and temporal variation of the temperature and optical intensity profiles provided that they incorporate the essential physics. Gain saturation in particular has been shown to have a significant effect on instability onset [5]. Furthermore, thermal lensing can significantly change the effective index profile of the fiber thus significantly changing the guided mode properties even to the point of changing an anti-guiding core into a guiding one [6]. These considerations suggest that a beam propagation model incorporating local population rate equations and capable of treating both transient and steady-state cases should be used to study the onset of instability.

Numerical models of instability should be able to describe the essential features observed in experiments. These include the onset threshold and the time dependent behavior of the output. It is challenging to predict thresholds using models that rely on the presence of noise due to the requirement to characterize the noise source. One notable exception is quantum shot noise which remains consistent in behavior. It may be argued that the threshold in the presence of shot noise is the highest physically-realistic value and that predictions of higher thresholds that do not account for this noise term are meaningless. Thresholds predicted in the absence of noise terms have been significantly higher than those predicted in the presence of noise or offset frequencies [4, 9]. Furthermore, simulated thresholds are mostly higher than experimentally observed ones although this may be partially due to the differences between the characteristics of the amplifiers studied. Most low-threshold experimental studies of instability have been conducted with counter-pumped amplifiers. Modeling of this configuration is complicated by the possible effect of mode coupling on the pump intensity at the seeded end. Furthermore, many experimental studies have been carried out with advanced higher order mode suppressing fiber designs that can be challenging to faithfully treat in numerical models.

The temporal characteristics of instability are examined most easily in the frequency domain. Time-dependent amplifier output characterization may be performed using modal decomposition techniques or with high-speed cameras or

Fiber Lasers XI: Technology, Systems, and Applications, edited by Siddharth Ramachandran,
Proc. of SPIE Vol. 8961, 89611U · © 2014 SPIE · CCC code: 0277-786X/14/$18
doi: 10.1117/12.2038648

aperture-enabled photodetectors. The frequency spectrum of the resulting time series may then exhibit peaks at well-defined frequencies. These may be characterized by their relative amplitudes, their widths, and the evolution of these characteristics as amplifier operating conditions are changed [10].

Recently, a new model capable of treating both periodic and non-periodic instability was published [7]. This model employs a fast hybrid harmonic finite-element non-linear scalar beam propagator with a triple hybrid harmonic finite element finite difference thermal solver. The beam propagation implementation enables treatment of thermal lensing and the adiabatic changes it causes to the waveguide in addition to stronger non-adiabatic perturbations. This model also incorporates heating through rate equation solutions based on the local signal and pump intensities. Thus it enables examination of the time behavior of the optical fields and temperature distribution throughout amplifiers exhibiting instability. Other researchers have suggested numerical tests of models that predict instability in the absence of frequency shifted modes suggesting that numerical noise amplified through STRS may be the cause of this observed instability. This implies that if realistic frequency-shifted seeding conditions including quantum noise or spontaneous thermal Rayleigh scattering (SpTRS) are included, the observed threshold should prove to be lower than that predicted without frequency-shifted input. This would support the claim that amplification of frequency-shifted light is the sole physical explanation for experimentally-observed instability [8]. Examination of the intensity fluctuation spectrum along the length of the fiber should then reveal the emergence of frequency-shifted components as the signal is amplified.

This work reports on the fluctuation spectrum of the intensity probes along the fiber and at the output calculated using a symmetric version of the model described above for different seeding conditions including a superposition of non-frequency-shifted transverse modes, quantum noise-seeded, and frequency-shifted fundamental and higher order modes.

2. MODELING APPROACH

The simulation of modal instability requires a fiber amplifier model that treats the propagation, interference, and amplification of multiple transverse modes, intermodal scattering by thermally induced refractive index changes, and time dependent evolution of the temperature distribution as a result of quantum defect heat loading. One assumption required for the model is that the temperature profile remains approximately static during the time it takes for the signal to propagate the length of the amplifier. This is reasonable because the optical time of flight is on the order of nanoseconds while the thermal response time is on the order of milliseconds, a difference of six orders of magnitude. Similarly, for a given pump and signal intensity, the response of the energy level populations within the optically active medium is assumed to be instantaneous. If a model were to attempt to take into account the slight temperature change that occurs during the optical propagation or energy level population transients, the time step required would be too small to allow a meaningful duration of time to be simulated.

Once this approximation is established, it becomes evident that the amplifier may be simulated by alternately updating the optical fields and temperature distribution as each affects the other: the optical fields determine the local optical intensity within the fiber which determines the quantum heat loading distribution leading to the temperature distribution while the temperature distribution affects the optical profiles directly through the thermo-optic effect. This general approach was first adopted because it was apparently the only one which allowed the treatment of longitudinal heat flow [3]. It has been subsequently argued that this has little if any effect on instability in amplifiers. Neglecting longitudinal heat flow opens up the possibility of determining the optical and temperature profiles for all time sequentially at each position along the direction of propagation as well as with the additional assumption of periodic boundary conditions in time [1,5,8,9].

Some care is required in applying the alternating thermal and optical updates. In the optical case there are several methods of obtaining the fields along the fiber given the fields at the input. In addition to the signal propagating in the core, the pump absorption in the cladding must also be calculated. It is convenient to use the same set of grid points for all of the properties characterizing a local point within the amplifier: signal intensity, pump intensity, population inversion, heat loading, and temperature. Thermal conductivity, doping concentration, mass density, and heat capacity are all assumed to be constant. In this case, however, the approximations of the derivatives describing the wave propagation accumulate additional error because the longitudinal average gain through the propagation step is systematically different than the value available at the starting end.

This situation is the motivation behind Runge-Kutta methods in solving sets of ordinary differential equations. Indeed coupled mode theory-based propagation schemes reduce to just such sets of equations to which Runge-Kutta methods

are often applied. The beam propagation method applied for the present work is similar in spirit although it includes the application of an implicit update step. The fields are propagated from one step to the next using the field values at the beginning of the step. The obtained values are then used to update the second half of the propagation step. In each case the first half-step is performed using an explicit updating scheme while the second half-step uses an implicit update.

A similar situation is encountered in the case of the time step update of the temperature distribution. If the heat distribution at a point in time is used to update the temperature distribution (which then changes the heat distribution through the thermo-optic effect) then the average heat distribution throughout the time step is different than that at the beginning. To overcome this, the same approach is adopted as in the optical propagation case. The heat distribution is calculated at the end of the time step and this distribution is then used to repeat the second half-step of the temperature update. This approach requires that the optical beam propagation be carried out throughout the entire amplifier length twice and that one explicit temperature update and two implicit updates be performed for each time step update. Each optical propagation step similarly requires one explicit update and two implicit updates. Therefore, the bulk of computational time is spent performing the implicit optical updates, four per time step per longitudinal step, which requires the solution of a sparse linear system. For the solutions presented here, 5158 longitudinal steps were used for 3300 time steps resulting in the requirement to accomplish about 68 million linear solves.

The time required to accomplish each linear solve increases with the size of the matrices therefore it is beneficial to find an efficient basis with which to express the optical fields. The basis used here combines a radial discretization over an arbitrary set of points with an azimuthal harmonic expansion. This approach combines the ability of finite element or finite difference schemes to treat arbitrary intensity distributions with the ability of modal decomposition schemes to effectively represent propagating modes with very few degrees of freedom. It takes direct advantage of the approximate azimuthal uniformity of large mode area fibers. The use of possibly non-uniform radial grids paves the way for future analysis of fibers with more complicated structures such as large pitch photonic crystal fibers and leakage channel fibers.

The azimuthal expansion previously reported enabled the general treatment of non-symmetric intensity profiles. In a great deal of cases, amplifiers have at least one mirror plane of symmetry and sometimes two. The interference of the fundamental LP_{01} and first higher order LP_{11} mode that plays the dominant role near threshold is faithfully represented with one plane of symmetry. This is implemented through the expansions

$$E(r,\varphi,z) = \sum_{q=0}^{Q} E_q(r,z)\cos\left[iq\varphi\right] \tag{1a}$$

$$n^2(r,\varphi,z) = n_0^2 + \sum_{q=0}^{Q} V_q(r,z)\cos\left[iq\varphi\right] \tag{1b}$$

of the electric field E and the refractive index n in a cylindrical coordinate system. The observation that the effects of modal instability are more severe in weakly-guiding large mode area fibers justifies the use of the scalar approximation to the electromagnetic wave equation governing the evolution of E. With these minor substitutions the previously presented derivation [7] holds resulting in an optical matrix order of $N\cdot(Q+1)$ which is significantly smaller than the order for the non-symmetric case of $N\cdot(2Q+1)$ where N is the number of radial points in the optical region which extends a few multiples of the core radius beyond the core. Additional radial points that extend to the outer cladding boundary are included in the temperature calculation and in both cases the point spacing may vary.

3. SIMULATED AMPLIFIER PROPERTIES

The amplifiers simulated here are based on large mode area cladding-pumped step-index Ytterbium-doped fibers that are conduction cooled to maintain a constant uniform temperature on the cylindrical outer cladding boundary. The amplifiers are assumed to be maintained in a straight configuration without bending or coiling. Table 1 summarizes amplifier parameter values used for the simulations. The main differences between the runs presented are the pumping power levels, the direction of the launched pump (co-pumped vs. counter-pumped), and the temporal properties of the seed.

The azimuthal order of the fields here is restricted to 4 while the radial discretization allows any radial order. It is important to reiterate that the modes are used for seeding the amplifier as well as decomposing the output but not for the

propagation. Figure 1 shows the first 9 modes for this fiber in the absence of thermal lensing. The first 7 modes are truly guided while the last two can be considered cladding modes. The 7th mode, LP_{41} represents the highest azimuthal order retained. The calculated propagation constants of these modes were compared to those obtained with the non-symmetric method as a check on the implementation and found to be identical. In the absence of symmetry, each of the modes with an azimuthal order greater than zero has a degenerate mode oriented on the other Cartesian axis. Other amplifier parameters are given in Table 1.

Table 1. Simulated Fiber Parameters

Parameter	Value
core diameter	74 μm
pump cladding diameter	170 μm
outer cladding diameter	170 μm
core numerical aperture	0.03
fundamental mode field area	2750 μm^2
beat length LP_{01}-LP_{11}	22.3 mm
fiber length	1.15 m
yb^{+3} doping concentration	3.5×10^{25} m^{-3}
signal wavelength	1.064 μm
pump wavelength	0.977 μm
signal power LP_{01}	varies
signal power LP_{11}	varies
pump power	varies
output power	varies
signal emission cross-section	3.58×10^{-25} m^2
signal absorption cross-section	6.00×10^{-27} m^2
pump emission cross-section	1.87×10^{-24} m^2
pump absorption cross-section	1.53×10^{-24} m^2
upper state lifetime	850 μs
thermal conductivity	1.38 W/m-K
heat capacity	703 J/kg-K
mass density	2201 kg/m^3
thermo-optic coefficient	1.2×10^{-5} K^{-1}
heat sink temperature	300 K
z grid spacing	2.23×10^{-4} m
time step	4.0×10^{-5} s
total simulation time	varies
thermal radial points	66
optical radial points	56
doped core radial points	29
optical azimuthal order	4
thermal azimuthal order	4

4. AMPLIFIER SEED CHARACTERISTICS

Studying the behavior of amplifiers with different seed source characteristics may provide insight into factors affecting instability onset. One key question is whether instability occurs in an amplifier in the absence of a frequency shifted noise term. Four types of initial seeding conditions are considered here: Seeding with the fundamental mode only, seeding with the fundamental and a higher order mode at the same frequency, seeding with the fundamental mode and a frequency-shifted higher order mode, and seeding with the fundamental mode and a higher order mode taking into account the quantum shot noise that each experiences.

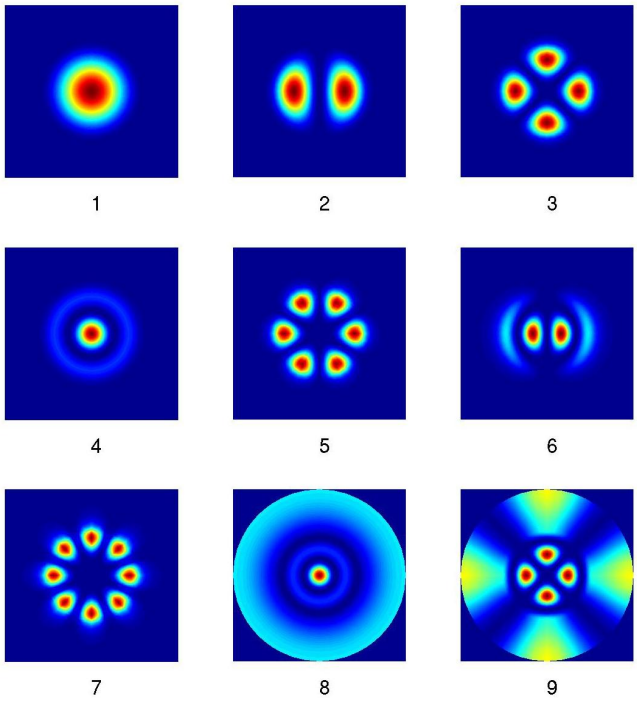

Figure 1. Field intensity plots for the first 9 guided modes of the fiber considered here in descending order of effective index: LP_{01} (1), LP_{11} (2), LP_{21} (3), LP_{02} (4), LP_{31} (5), LP_{12} (6), LP_{41} (7), and 8 and 9 are cladding modes.

Seeding with any number of modes with any power levels requires only setting the initial fields at the beginning of the beam propagation through superposition. This initial condition then remains constant throughout the time evolution of the amplifier. The initial relative phase of the modes will set the starting phase of the interference pattern among the modes. Introducing a frequency shift between two of the modes is accomplished by changing the relative phase between the modes in time at a constant rate throughout time. The initial field is then given by

$$E(r,\varphi,z=0)=\sqrt{P_0}\psi_0\left(r,\varphi\right)+\exp\left[i\Delta\omega t\right]\sqrt{P_1}\psi_1\left(r,\varphi\right) \tag{2}$$

for two launched modes where $P_{0,1}$ are the modal powers launched, $\psi_{0,1}\left(r,\varphi\right)$ are the normalized mode field distributions, and $\Delta\omega$ is the frequency difference between the two launched modes. This changes the interference pattern leading to travelling intensity and temperature gratings, the latter lagging the former. Setting $\Delta\omega=0$ leads to the initial condition for the non-frequency-shifted case.

The case of quantum shot noise seeding is interesting in that it may set the upper limit on the instability threshold. This noise term results from the Poisson statistics governing the emission of photons from the seed source of the amplifier. Assuming that it is a laser oscillator, its rate equations govern the average rate of stimulated emission but the precise times that the photons are emitted is random leading to a very small uncorrelated amplitude modulation for each launched mode. This noise source is physically unavoidable, although in theory it can be reduced through extraordinary measures such as employing a squeezed-light seed source.

Poisson statistics are described by the rule that the uncertainty in the number of photons entering the amplifier in any given time interval is equal to the square root of the number of photons

$$\delta n=\sqrt{n}. \tag{3}$$

Considering the number of photons at frequency ν incident during a time interval Δt at a given seed power level P leads directly to an expression for the width of the power distribution function

$$\sigma_P = \sqrt{\frac{Phv}{\Delta t}}. \tag{4}$$

where h is Planck's constant. For signal wavelengths near 1.064 microns and a power level of 15 Watts this works out to approximately $\sigma_P = 2\times10^{-7}$ Watts evenly spread across all frequencies. For large numbers of photons, the Poisson distribution is well approximated by the normal Gaussian distribution. To implement the power spread in the model, a normally-distributed random number is generated at each time step to determine the amount of power to add or subtract from the initial condition for each mode according to Equation (4).

5. RESULTS

5.1 Co-pumped Amplifier

The large amount of data generated during the amplifier simulations requires a choice of which to keep and analyze. Storing the optical field at each propagation step for each time step would require about 72 GB and the same for the temperature profile. Instead, the full optical output field at each time step is recorded as well as the three components of the optical state vector required to calculate the optical intensity at the center of the fiber and at a point offset from the core to first azimuthal order for all propagation steps and all time steps.

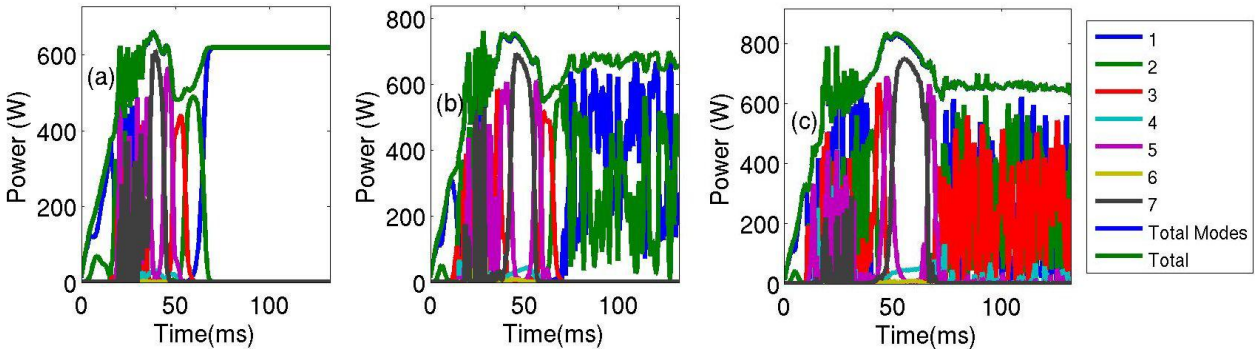

Figure 2. Evolution of the output modal composition of co-pumped amplifiers in time. The launched pump powers were (a) 700 Watts, (b) 800 Watts, and (c) 900 Watts. The launched seed contained 15.0 Watts in the fundamental mode and 0.75 Watts in the first higher order mode with no frequency shift between them. The modal decomposition is relative to the cold fiber modes identified in Figure 1.

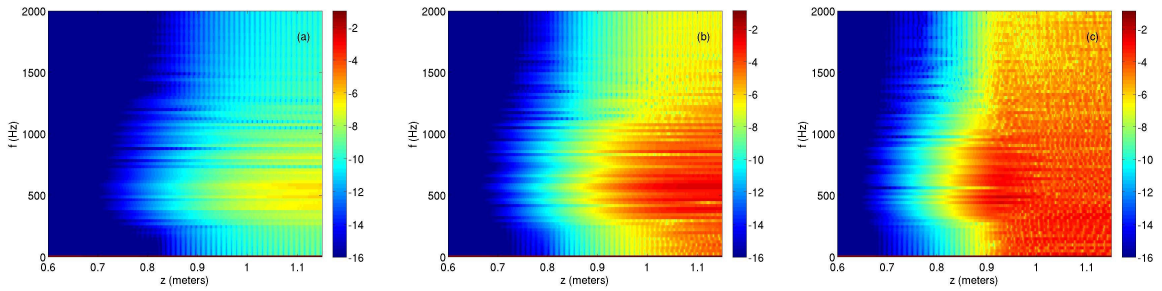

Figure 3. Evolution of the logarithmic frequency spectrum of the off-center optical intensity probe along the length of the co-pumped amplifier for the case of seeding with two modes and no frequency offset. The probe is located one-third of the core radius off the center in the horizontal direction in the reference frame of Figure 1 and includes only the lowest two azimuthal terms. The launched pump powers are the same as those depicted in Figure 2.

The first set of results presented concerns a co-pumped amplifier seeded with 15.0 Watts in the fundamental mode and 0.75 Watts in the first higher order mode (Mode 2 in Figure 1) and with no quantum shot noise or frequency-shifted input. Three launched pump powers are depicted: 700, 800, and 900 Watts corresponding to below, near, and well above threshold. For the 700 Watt case, the output power was 619 Watts, but for the other two cases the output power fluctuated significantly. Various definitions of the modal instability threshold have been presented in the literature.

Precisely applying one of these definitions requires fine tuning the pump power over a number of computational runs with very similar parameters. For this work, estimates of the thresholds are made based on the visibility of output fluctuations on full-range plots such as those shown in Figure 2. The instability threshold for this first set of parameters is estimated from these results to be between 619 and 675 Watts.

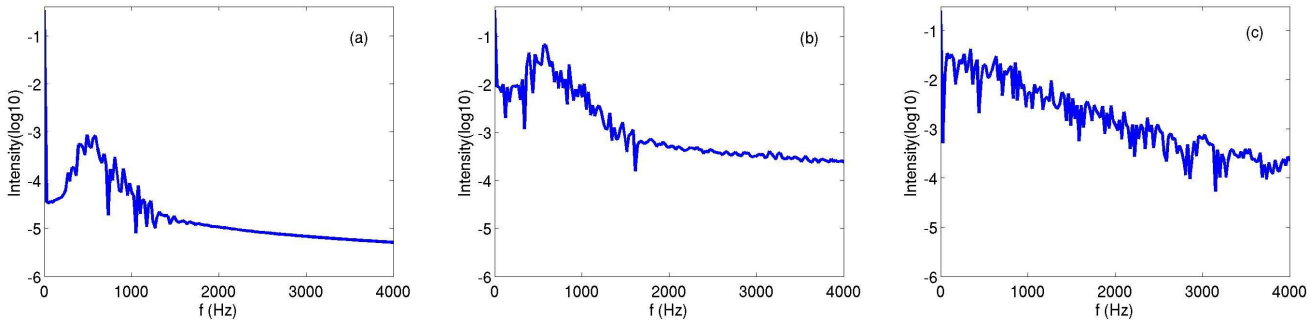

Figure 4. Output frequency spectra incorporating all azimuthal orders for the offset probe. The launched pump powers are the same as those depicted in Figure 2.

In each case the seed was held constant while the pump was ramped linearly from zero to its maximum value over a time period of 20 milliseconds. Figure 2 shows the evolution modal content of the amplifier output in time. Shortly after turn on, each case exhibits a transient region as the optical length of the amplifier grows toward its equilibrium value as it heats up. After approximately 70 milliseconds the transients are complete and the long-time behavior of the amplifier sets in. For the purposes of spectral analysis, only the time period after 91 milliseconds is included which amounts to 1024 time steps or 41 milliseconds. The fast Fourier transform was taken over these last 41 milliseconds to determine the frequency spectrum of the intensity probe offset from the fiber center.

It is interesting to note that Figure 2(a) shows no sign of instability after the transient regime but Figure 3(a) and 4(a) describing the same operating condition reveals the build-up of a non-zero spectral component. The 800 Watt pumping case depicted by Figures 2(b), 3(b), and 4(b) exhibits the most well-defined spectral peak at a frequency offset of -561 Hz with the frequency of the higher order mode content being generated less than the frequency of the fundamental mode by this amount. The 900 Watt pumping case (Figures 2(c), 3(c), and 4(c)) exhibits a broad frequency spread with no well-defined peaks and coupling between many of the higher order modes. The observation that the traces corresponding to the total output power obtained by integrating the intensity over the aperture (labeled "Total" in the plot legend) and the sum of the modal powers (labeled "Total Modes" in the plot legend) overlay well indicates that the thermally-induced distortions are not scattering power out of the set of the first 7 modes.

It is also interesting to note that the instability spectrum range in the few hundred Hertz to few kHz is smaller than the spectral linewidth of even single longitudinal mode seed sources which may be related to the apparent lack of dependence of the instability threshold on the linewidth of the seed source [3].

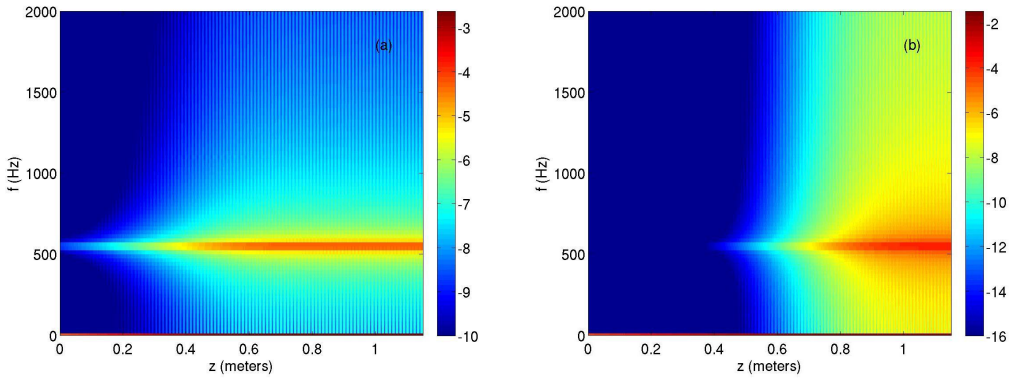

Figure 5. Evolution of the logarithmic frequency spectrum of the off-center optical intensity probe along the length of the co-pumped amplifier for the case of seeding primarily with the fundamental mode (15 Watts) with a very small amount of power in the first higher order mode (1.0 mW (a) and 1.0E-16 W (b)) with a frequency shift of -550.0 Hz.

The next set of results concerns seeding with the fundamental LP_{01} mode and the frequency-shifted LP_{11} mode. Two power levels were used for the LP_{11} mode: 1 milliwatt, and 1×10^{-16} Watts. The choice of the former was somewhat arbitrary. The choice of the latter value was motivated by arguments put forth by other researchers [9] that this is a good estimate of the level generated by quantum fluctuations for conservative instability threshold determinations.

Qualitatively the results are very similar with the frequency-shifted component growing rapidly along the length of the fiber and remaining spectrally pure as seen in Figure 5. The main difference between the two cases is that with the larger seed power, an appreciable amount of power ends up in the higher order mode with a pump power of only 100 Watts and an output of 97 Watts (at this low pump power the launched seed accounts for a noticeable fraction of the output power) which is shown in Figure 5(a). With the smaller seed power the threshold occurs at a pump power of about 410 Watts and a total output of 374 Watts. The modal decomposition of the output confirms that the observed fluctuations are due to coupling from the fundamental LP_{01} mode to the LP_{11} higher order mode.

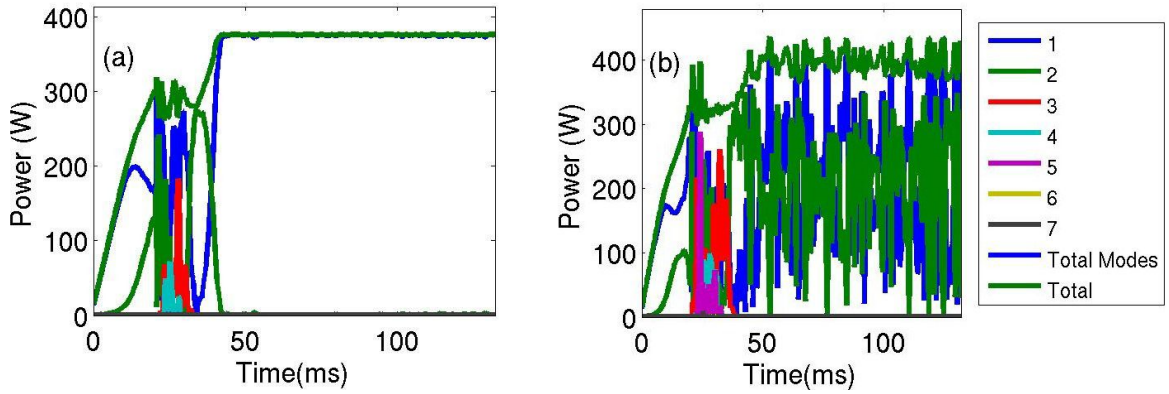

Figure 6. Evolution of the output modal composition of the co-pumped amplifier in time. The launched pump powers were (a) 410 Watts, and (b) 480 Watts. The launched seed had 15.0 Watts in the fundamental mode and 0.75 Watts in the first higher order mode with quantum shot noise.

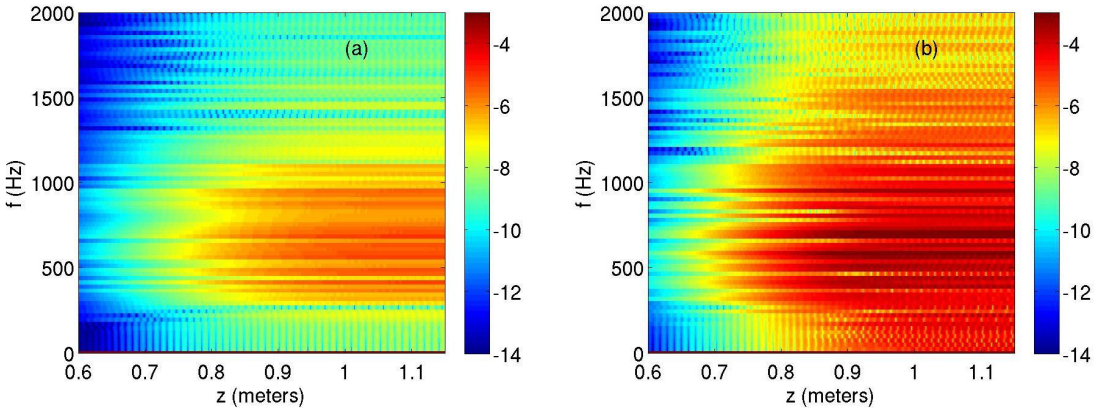

Figure 7. Evolution of the logarithmic frequency spectrum of the off-center optical intensity probe along the length of the co-pumped amplifier for the cases shown in Figure 6.

The next set of results implements quantum shot noise seeding as described in the previous section. Figure 6(a) shows the output modal decomposition near the instability threshold. The pumping power is 410 Watts and the seed has 15.0 Watts of power in the fundamental mode and 0.75 Watts of power in the LP_{11} mode each with quantum shot noise. This results in a total output power of 376 Watts. Figure 6(b) shows the output with 480 Watts of pumping which is significantly above threshold. At this power level all of the power couples back and forth between the first two modes in a non-periodic fashion. This is to be expected since the shot noise is non-periodic. Nevertheless a broad frequency peak develops with a center near -600 Hz. As the pump power is increased from 410 to 480 Watts, the peak broadens and the low frequency valley fills in as shown in Figures 7 and 8.

To summarize the different threshold values obtained for the co-pumped amplifier: with quantum shot noise seeding and a seed of 1×10^{-16} frequency shifted to the value for maximum stimulated thermal Rayleigh scattering gain the threshold powers were 376 and 374 Watts respectively. In the absence of shot noise or a frequency shift the threshold was well above 600 Watts, however, the instability spectrum was characterized by a peak similar to the one that developed in the case of quantum shot noise seeding.

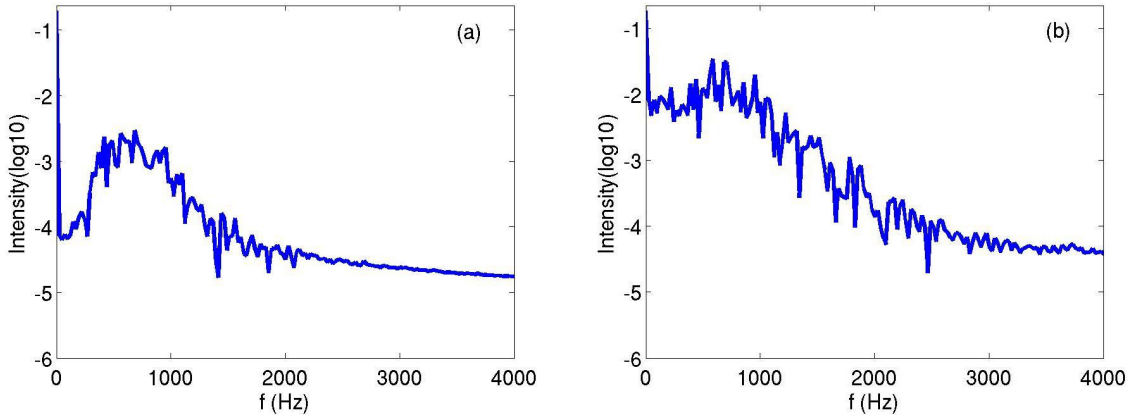

Figure 8. Output frequency spectra incorporating all azimuthal orders for the offset probe. The launched pump and seed powers are the same as those depicted in Figure 6.

5.2 Counter-pumped amplifier

The first results presented for the counter-pumped amplifier are for the case of quantum noise seeding. The output residual pump power was ramped on linearly at the beginning of the runs so that the total output power rises sharply at first and then begins to level off before reaching maximum power 20 milliseconds into the run. Figure 9 shows the modal composition of the output just below and well above the threshold.

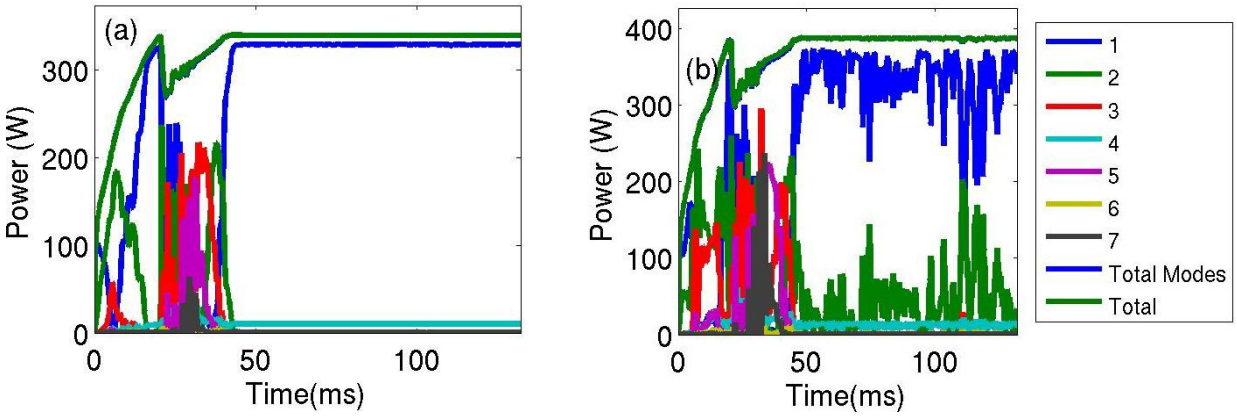

Figure 9. Evolution of the output modal composition of the counter-pumped amplifier in time. The launched pump powers were (a) 380 Watts, and (b) 438 Watts. The launched seed had 15.0 Watts in the fundamental mode and 0.75 Watts in the first higher order mode with quantum shot noise.

The first pumping power (Figure 9(a), 10(a), and 11(a)) was 380 Watts generating an output of 340 Watts. Ripples in the modal content are barely visible at the scales used for Figure 9(a). In both Figures 9(a) and 9(b), a noticeable component of the first axisymmetric higher order mode appears due to strong thermal lensing present due to the higher concentrated heat load in the counter-pumped case.

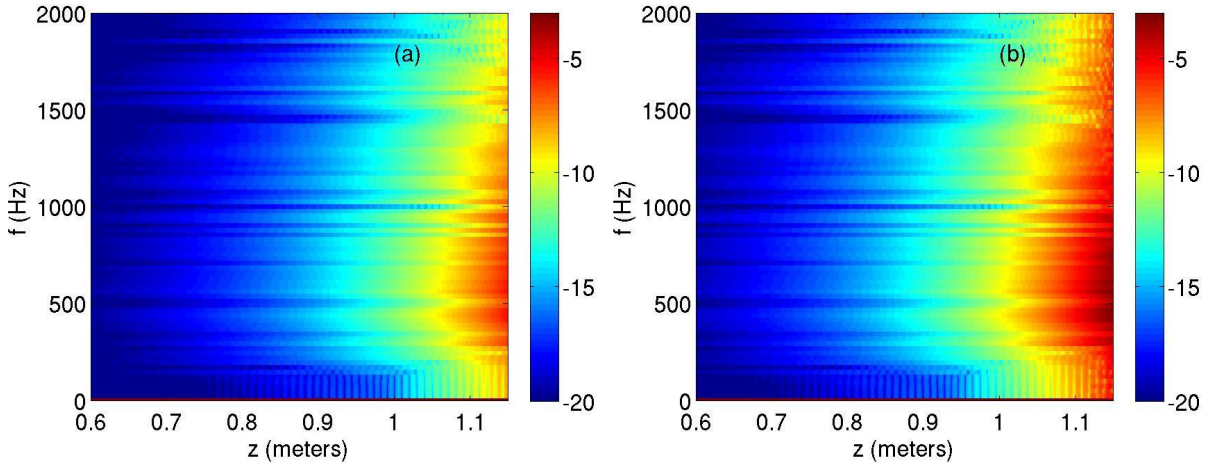

Figure 10. Evolution of the logarithmic frequency spectrum of the off-center optical intensity probe along the length of the counter-pumped amplifier for the cases shown in Figure 9.

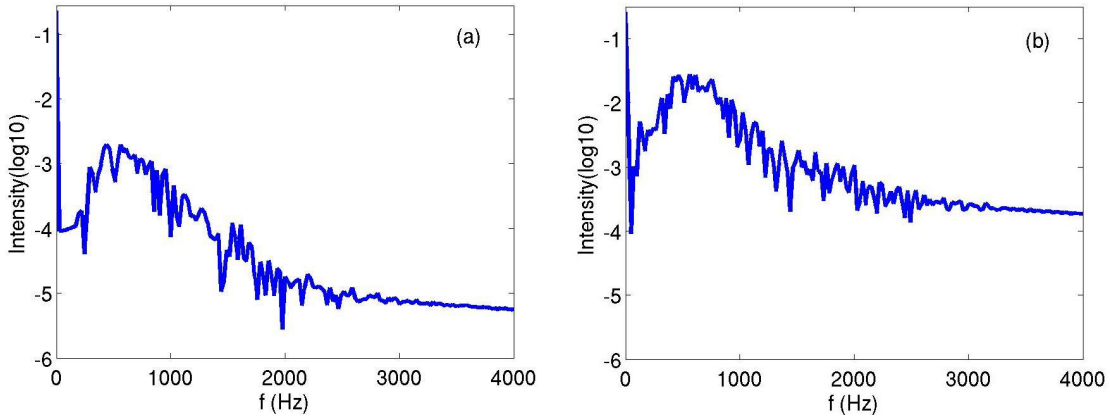

Figure 11. Output frequency spectra incorporating all azimuthal orders for the offset probe. The launched pump and seed powers are the same as those depicted in Figure 9.

While the modal fluctuations shown in Figure 9(b) are much stronger than those in 9(a), the Fourier spectra are remarkably similar in shape exhibiting a broad peak centered again near -600 Hz as seen in Figures 10 and 11.

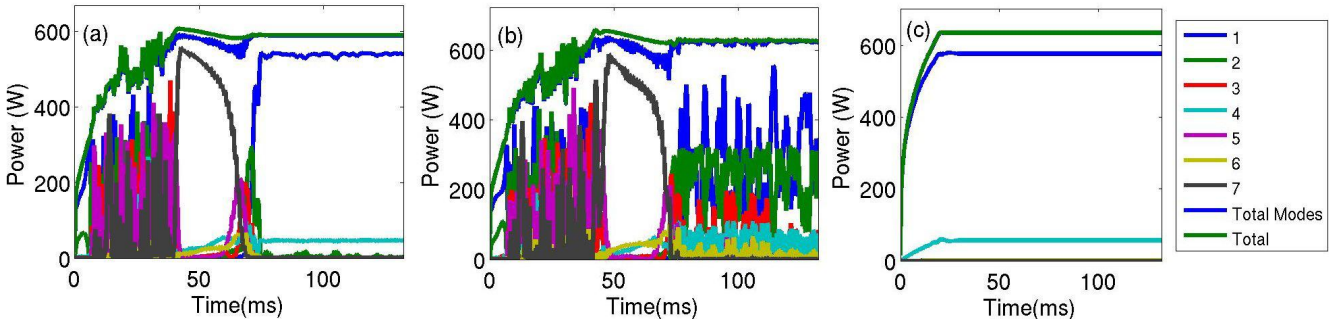

Figure 12. Evolution of the output modal composition of the counter-pumped amplifier in time. The launched pump powers were (a) 710 Watts, (b) 764 Watts, and (c) 774 Watts. The launched seed had 15.0 Watts in the fundamental mode and 0.75 Watts in the first higher order mode for (a) and (b), and 15.75 Watts in the fundamental mode for (c) with no quantum shot noise.

The final set of results concerns the counter-pumped amplifier with no quantum noise seeding. The instability threshold is about 589 Watts in this case when the amplifier is seeded with 15 Watts of LP_{01} and 0.75 Watts of LP_{11}. In order to assess the effect of the higher order mode with no frequency shift, the amplifier was simulated both with (Figures 12(a) and 12(b)) and without (Figure 12(c)) power launched into the LP_{11} mode. Figure 12(a) shows the modal output powers as a function of time below threshold, 12(b) shows the same above threshold, and 12(c) shows below-threshold operation without any LP_{11} component in the seed. Although it appears that there is no sign of instability in Figure 12(c), the Fourier spectra shown in Figures 13(c) and 14(c) corresponding to this case exhibits a weak but noticeable peak at -415 Hz.

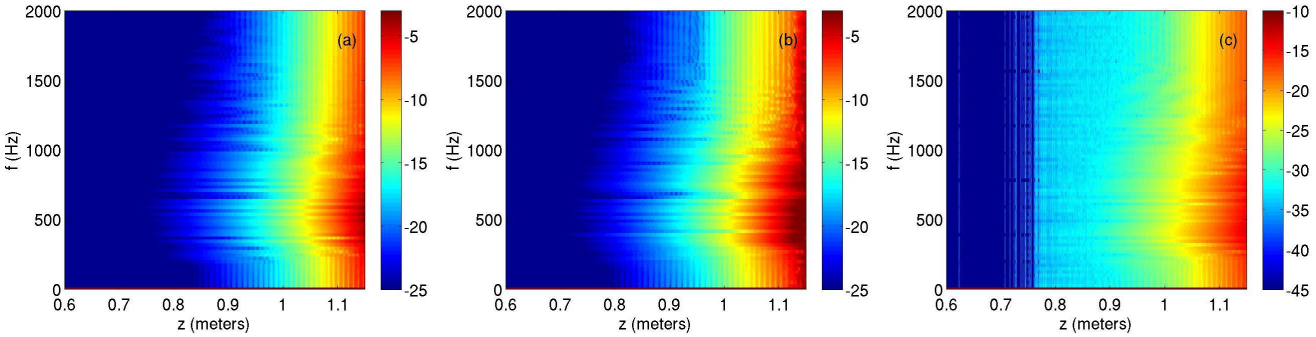

Figure 13. Evolution of the logarithmic frequency spectrum of the off-center optical intensity probe along the length of the counter-pumped amplifier for the cases shown in Figure 12.

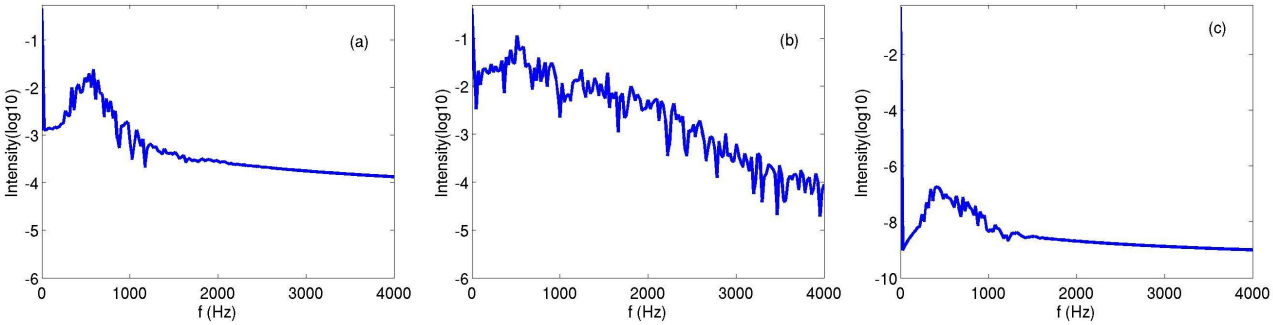

Figure 14. Output frequency spectra incorporating all azimuthal orders for the offset probe. The launched pump and seed powers are the same as those depicted in Figure 12

Table 2. Shows a summary of the results presented above including seeding conditions, pumping conditions, threshold values, frequency of the Fourier spectrum peak near threshold, and the figure reference.

Table 2. Summary of Results

Pumping Direction	Seed Noise	Threshold	Spectral Peak	Figures
Co-pumping	none	619-675 W	-561 Hz	2-4
Co-pumping	single-frequency (1E-3 W)	100 W	-550 Hz	5
Co-pumping	single-frequency (1E-16W)	374 W	-550 Hz	5
Co-pumping	quantum shot noise	376 W	-561 Hz	6-8
Counter-pumping	quantum shot noise	365 W	-561 Hz	9-11
Counter-pumping	none	589 W	-586 Hz	12-14

6. DISCUSSION AND CONCLUSION

Results have been presented for numerical simulations of the dynamic behavior of fiber amplifiers experiencing modal instability. These were aimed at investigating the possibility that different proposed instability mechanisms occurred under different amplifier conditions. The fiber properties for all of the simulations were kept the same while the pumping and seeding conditions were varied. Co- and counter-pumping arrangements were simulated at a range of powers in the vicinity of the instability threshold. Additionally, three relevant seeding conditions were simulated: ideal, noiseless seeding, seeding that includes quantum shot noise, and frequency-shifted seeding.

If instability is indeed noise-induced, the case of quantum shot noise seeding arguably determines the maximum threshold for a given amplifier. If instability is not noise-induced, then the absence or presence of noise in the input should have little effect on the instability threshold or behavior. Introducing frequency-shifted higher order modes, while mathematically justified by arguments centering on the narrowness of the STRS gain spectrum and the presence of spontaneous thermal Rayleigh scattering, seems somewhat removed from actual operating conditions. On the other hand quantum shot noise is very well understood and does not favor any particular range of frequencies.

At first it would seem that instability observed in a simulation in the absence of noise would confirm an alternate instability mechanism, however, an explanation has been provided that takes into account unavoidable numerical noise due to the finite precision of numerical calculations [8]. It could then be the case that the STRS process amplifies the numerical noise leading to the instability observed in the noiseless simulations. Estimates of the noise equivalent power due to truncation error predict that numerical noise seeded instability thresholds should be higher than quantum noise seeded thresholds. This hypothesis is consistent with the results presented here. This leads to the question of whether the threshold in the absence of higher order mode seeding shown in Figure 12(c) should have been roughly the same as in its presence. The answer to this question requires consideration of the particular characteristics of numerical noise as related to the hybrid azimuthal field expansion. Since the higher azimuthal terms are identically zero for the fundamental mode, multiplication by zero in the beam propagation may retain higher precision leading to the observed higher threshold.

Gain curves for STRS in large mode area fibers have been published [11,12] and the STRS gain peak for this particular fiber has independently been determined to be near -550 Hz [13]. The peaks in the output spectra for all of the amplifier configurations examined here all fall near this value. It was found to be of the utmost importance to allow at least 90 milliseconds from the beginning of the simulations for transients to decay before calculating the output spectra. These results suggest that STRS amplification of included noise or numerical noise is responsible for the observed modal instability. These limited results do not preclude other mechanisms for other types of fibers. There may remain different operating regimes in which alternate instability mechanisms operate. These results do support the view that reducing the STRS gain should be an effective way of raising the instability threshold of fiber amplifiers.

ACKNOWLEDGEMENTS

This work was made possible by a grant of computing time at the U S. Army Engineer Research and Development Center and Air Force Research Laboratory Department of Defense Supercomputing Resource Centers from the U. S. Department of Defense High Performance Computing Modernization Program. This work was supported by the United States Air Force Academy Department of Physics Laser and Optics Research Center and the US Department of Defense High Energy Laser Joint Technology Office under the Multidisciplinary Research Initiative “Fiber Laser Light Engines.” The author would like to thank Arlee and Jesse Smith for helpful discussions. The views expressed in this article are those of the author and do not reflect the official policy or position of the US government or the Department of Defense. Distribution A: Approved for public release, distribution unlimited.

REFERENCES

[1] A. V. Smith and J. J. Smith, “Mode instability in high power fiber amplifiers,” Opt. Express 19, 10180–10192 (2011).

[2] C. Jauregui, T. Eidam, H. Otto, F. Stutzki, F. Jansen, J. Limpert, and A. Tünnermann, “Physical origin of mode instabilities in high-power fiber laser systems,” Opt. Express 20, 12912-12925 (2012).

[3] B. Ward, C. Robin, and I. Dajani, "Origin of thermal modal instabilities in large mode area fiber amplifiers," Opt. Express 20, 11407-11422 (2012).
[4] S. Naderi, I. Dajani, T. Madden, and C. Robin, "Investigations of modal instabilities in fiber amplifiers through detailed numerical simulations," Opt. Express 21, 16111-16129 (2013).
[5] A. V. Smith and J. J. Smith, "Increasing mode instability thresholds of fiber amplifiers by gain saturation," Opt. Express 21, 15168-15182 (2013).
[6] F. Jansen, F. Stutzki, H. Otto, C. Jauregui, J. Limpert, and A. Tünnermann, "High-power thermally guiding index-antiguiding-core fibers," Opt. Lett. 38, 510-512 (2013).
[7] Benjamin G. Ward, "Modeling of transient modal instability in fiber amplifiers," Opt. Express 21, 12053-12067 (2013).
[8] A. V. Smith and J. J. Smith, "Review of models of mode instability in fiber amplifiers," http://www.as-photonics.com/publications/FiberLaser/Model_review.pdf, accessed 7/3/2013.
[9] A. V. Smith and J. J. Smith, "Influence of pump and seed modulation on the mode instability thresholds of fiber amplifiers," Opt. Express 20, 24545-24558 (2012).
[10] M. M. Johansen, M. Laurila, M. D. Maack, D. Noordegraaf, C. Jakobsen, T. T. Alkeskjold, and J. Lægsgaard, "Frequency resolved transverse mode instability in rod fiber amplifiers," Opt. Express 21, 21847-21856 (2013).
[11] K. R. Hansen, T. T. Alkeskjold, J. Broeng, and J. Lægsgaard, "Theoretical analysis of mode instability in high-power fiber amplifiers," Opt. Express 21, 1944-1971 (2013).
[12] L. Dong, "Stimulated thermal Rayleigh scattering in optical fibers," Opt. Express 21, 2642-2656 (2013).
[13] J. J. Smith, private communication, 11 June 2013 – 14 November 2013.